J Solid State Electrochem (2012) 16:3559–3571
DOI 10.1007/s10008-012-1787-3

ORIGINAL PAPER

Electrochemical behavior of $Li[Li_{0.2}Co_{0.3}Mn_{0.5}]O_2$ as cathode material in Li_2SO_4 aqueous electrolyte

K. C. Mahesh · G. S. Suresh · T. V. Venkatesha

Received: 13 April 2012 / Revised: 17 May 2012 / Accepted: 23 May 2012 / Published online: 8 June 2012

Abstract Layered, lithium-rich $Li[Li_{0.2}Co_{0.3}Mn_{0.5}]O_2$ cathode material is synthesized by reactions under autogenic pressure at elevated temperature (RAPET) method, and its electrochemical behavior is studied in 2 M Li_2SO_4 aqueous solution and compared with that in a non-aqueous electrolyte. In cyclic voltammetry (CV), $Li[Li_{0.2}Co_{0.3}Mn_{0.5}]O_2$ electrode exhibits a pair of reversible redox peaks corresponding to lithium ion intercalation and deintercalation at the safe potential window without causing the electrolysis of water. CV experiments at various scan rates revealed a linear relationship between the peak current and the square root of scan rate for all peak pairs, indicating that the lithium ion intercalation–deintercalation processes are diffusion controlled. The corresponding diffusion coefficients are found to be in the order of 10^{-8} cm^2 s^{-1}. A typical cell employing $Li[Li_{0.2}Co_{0.3}Mn_{0.5}]O_2$ as cathode and $LiTi_2(PO_4)_3$ as anode in 2 M Li_2SO_4 solution delivers a discharge capacity of 90 mA h g^{-1}. Electrochemical impedance spectral data measured at various discharge potentials are analyzed to determine the kinetic parameters which characterize intercalation–deintercalation of lithium ions in $Li[Li_{0.2}Co_{0.3}Mn_{0.5}]O_2$ from 2 M Li_2SO_4 aqueous electrolyte.

Keywords $Li[Li_{0.2}Co_{0.3}Mn_{0.5}]O_2$ · Cathode material · RAPET method · Intercalation–deintercalation process · Aqueous rechargeable lithium-ion cells

K. C. Mahesh · G. S. Suresh (✉)
Chemistry Research Centre, SSMRV Degree College,
Jayanagar,
Bangalore 560041, India
e-mail: sureshssmrv@yahoo.co.in

T. V. Venkatesha
Department of Chemistry, Kuvempu University,
Jnanasahyadri, Shankaraghatta,
577451 Shimoga, India

Introduction

Much interest has been placed on the layered $LiMnO_2$ compound for its prospects of providing not only a low-cost but also an environmentally benign cathode material for rechargeable lithium ion batteries [1, 2]. However, $LiMnO_2$ is not thermodynamically stable at elevated temperatures and thus cannot be synthesized by the same methods as those used for other layered compounds. One of the methods to stabilize the layered structure of $LiMnO_2$ is to make the electronic properties of manganese to be more cobalt-like by substitution of manganese with more electron-rich elements. Successful substitution of manganese by cobalt [3–5] and nickel [6–8] has been reported by many research groups. Bruce et al. [4, 9, 10] investigated the synthesis and electrochemical behavior of cobalt substituted $LiMn_{1-x}Co_xO_2$. The cycling behavior of these materials is much improved over the cobalt-free compounds [11]. Work on these cobalt substituted α-$NaFeO_2$ structure materials, where manganese is the redox active ion, has essentially ceased because of the inability to maintain the structure relative to conversion to the spinel structure under realistic cycling conditions.

Thackeray et al. [12] suggested that the lithium-rich compounds with layered structure show quite interesting electrochemical properties to the electrode material by improving structural stability by the formation of two component composite material like $xLi_2MnO_3(1-x)LiMO_2$ (M = Mn, Ni, Co, etc.) [12]. The solid solution series between Li_2MnO_3 ($Li[Li_{1/3}Mn_{2/3}]O_2$) and $LiMO_2$ have received significant attention as an alternative cathode material for $LiCoO_2$ due to their high discharge capacity. Li_2MnO_3 was considered electrochemically inactive because Mn^{4+} in Li_2MnO_3 normally could not be oxidized beyond 4+ oxidation state in order to extract lithium from its lattice. However, a substantial charge can be removed from, and, to some extent, reinserted into the Li_2MnO_3 structure. Lu and Dahn [13] have analyzed the solid solution

between Li_2MnO_3 and $LiMO_2$ (M = Ni or Cr), which can be regarded as $Li[Ni_xLi_{(1/3-2x/3)}Mn_{(2/3-2x/3)}]O_2$ and $Li[Cr_xLi_{(1/3-2x/3)}Mn_{(2/3-2x/3)}]O_2$. These oxides are derived from $Li[Li_{1/3}Mn_{2/3}]O_2$ by substitution of Li^+ and Mn^{4+} by Ni^{2+} or Cr^{3+}, respectively. The promising lithium-rich compounds such as $Li[Li_{1/3-2x/3}Mn_{2/3-x/3}M_x]O_2$ can deliver very high discharge capacity of 200–240 mA h g^{-1} between 2.0 and 4.8 V, and exhibit excellent cycling performance [13]. Despite their exceptional high capacity and low cost, $xLi_2MnO_3(1-x)LiMO_2$ materials suffer from two major disadvantages of low initial coulombic efficiency and poor rate capability, which bring about great difficulties for practical applications [14]. Although there has been no definite evidence presented so far, the large initial irreversible capacity loss is usually attributed to an irreversible removal of partial lithium as Li_2O along with an elimination of the oxygen vacancies from the crystal lattice produced during first charge, which lead to a reduction of the effective sites for accommodating the lithium ions in subsequent cycles [15]. Similarly, several mechanisms, such as the formation of a thick solid–electrolyte interface (SEI) on the cathode surface and the frustrated diffusion of lithium ions in the rearranged lattice formed during the first charge, have been proposed to account for the low rate capability of the $Li_2MnO_3LiMO_2$ materials, but the rapid capacity fading of the materials with increased charge and discharge rate is not fully understood [16–19].

On the other hand, lithium ion batteries, which offer outstanding technical performances concerning the available gravimetric energy density, are limited by several drawbacks such as severe safety problems, as well as economic and environmental problems [20, 21]. The flammable organic electrolytes used in lithium ion batteries may cause smoke or fire in the case of improper use such as overcharge or short circuit. Moreover, lithium ion batteries are expensive, because of the complicated cell designing, the necessity of a perfectly dry environment during some manufacturing steps and the costly non-aqueous electrolytes [22]. Overall, the economic and ecologic problems, with which present-day lithium ion batteries are concerned, continuously require the development of less expensive and "green" energy storage materials and devices. As an alternative, a new type of rechargeable lithium ion battery with an aqueous electrolyte was announced in the middle of 1990s [23–25]. This type of battery uses the lithium intercalation compounds as electrode materials and an aqueous electrolyte solution. By this combination, the disadvantages of the non-aqueous lithium battery, i.e., inflammability, toxicity, high cost and safety problems, can be avoided. Due to the aqueous electrolyte the cell voltage is restricted to about 1.3 V, the decomposition potential of water, in comparison to 3–4 V in organic electrolyte. As a consequence, only low energy density can be expected from this kind of battery but can be compared with that of Pb–acid and Ni–Cd batteries, which use toxic metals.

Many attempts have been made to synthesize lithium rich compounds through solid state process [26], sol–gel method [27, 28], polymer–pyrolysis method [14], co-precipitation method [29], combustion method [30], etc. Here, we report the use of $Li[Li_{0.2}Co_{0.3}Mn_{0.5}]O_2$, a solid solution of Li_2MnO_3 and $LiCoO_2$, obtained by Co substitution for Li and Mn in Li_2MnO_3, synthesized by reactions under autogenic pressure at elevated temperature (RAPET) method as cathode material in combination with $LiTi_2(PO_4)_3$ anode and 2 M Li_2SO_4 aqueous solution as electrolyte. RAPET method is a simple, one-stage, efficient, economic and scalable approach for the synthesis of a variety of materials. The process involves heating of precursors in a closed stainless steel cell. The average particle size and size distribution can be manipulated by controlling the temperature and duration of heating. The electrochemical properties of $Li[Li_{0.2}Co_{0.3}Mn_{0.5}]O_2$ in an aqueous electrolyte is studied and compared with that in an organic electrolyte.

Experimental

Stoichiometric amounts of LiOH, Co_3O_4 and MnO_2 (all from Sigma-Aldrich) are weighed to produce a 0.6-g product, and then mixed and ground well. The resulting powder is introduced into a 5-ml Swagelok. The Swagelok parts consist of a small threaded stainless steel tube closed by two caps from both sides. The filled Swagelok is closed tightly and then placed inside an alumina pipe in the middle of the furnace. The temperature is raised to 600 °C at a rate of 10 °C/min and held at this temperature for 14 h. The chemical dissociation and transformation reaction takes place under the autogenic pressure of the precursor at the fixed temperature. The Swagelok cell is allowed to cool gradually to room temperature, opened, and the obtained product is used after grinding. Crystalline $LiTi_2(PO_4)_3$ anode material was prepared in the same manner by heating a mixture of TiO_2, $NH_4H_2PO_4$ and LiH_2PO_4 in an appropriate molar ratio at 900 °C for 15 h and by cooling it slowly to room temperature.

Powder X-ray diffraction (XRD) patterns of the samples were recorded using a Philips X'pert Pro diffractometer with CuKα (λ=1.5418 Å) as the source. Electrodes were prepared using stainless steel mesh as a current collector. The mesh was cut into circular shape of about 1 cm^2 area and welded with stainless steel wire for electrical contact. The mesh was sandblasted to remove the oxide layer, washed with water, rinsed with acetone, dried and weighed. Cathode and anode materials were prepared in the same way. Powder mixture of the sample, carbon black and polyvinylidene fluoride (PVdF) in the weight ratio of 75:20:5 were ground in a mortar; a few drops of *N*-methyl-2-pyrrolidone (NMP) were added to obtain a slurry. The slurry was coated onto the pretreated mesh and dried in a vacuum oven at 110 °C overnight.

A three-electrode electrochemical cell was employed for CV in aqueous 2 M Li_2SO_4 solution. A saturated calomel electrode (SCE) and Pt foil were used as reference and counter electrodes, respectively. Galvanostatic charge–discharge measurements were carried out using coin-type cell consisting of $Li[Li_{0.2}Co_{0.3}Mn_{0.5}]O_2$ cathode and $LiTi_2(PO_4)_3$ anode. Electrochemical impedance measurements were carried out potentiometrically using a three-electrode system with an ac excitation signal of 10 mV over the frequency range 100 kHz–5 MHz. All experiments involving $Li[Li_{0.2}Co_{0.3}Mn_{0.5}]O_2$ in organic electrolyte were carried out in the same way. The test cell was prepared with Li metal foil as reference and counter electrodes, and a 1 M $LiAsF_6$ dissolved in EC+DMC (1:1 v/v) as the electrolyte solution. Celgard 2340 was used as the separator. Assembling of the cell was carried out in a glove box filled with argon gas. All electrochemical measurements were made using a Biologic potentiostat–galvanostat instrument.

Results and discussion

Physical characterization

XRD technique was employed to evaluate the crystal structure of the synthesized materials obtained by RAPET method. Figure 1a shows the XRD pattern of $Li[Li_{0.2}Co_{0.3}Mn_{0.5}]O_2$ compound prepared by RAPET method at 600 °C for 14 h. All strong diffraction lines can be indexed as a layered oxide lattice based on a hexagonal α-$NaFeO_2$ structure with a space group *R3m* and show very sharp peaks, indicating a high degree of crystallinity. The weak peaks between 20° and 25° are reflected by a monoclinic unit cell with a *C2/m* symmetry rather than a *R3m* lattice, due to a $LiMn_6$ cation arrangement that occurs in the transition metal layers of Li_2MnO_3 regions [14]. Therefore, the layered $Li_{1+x}MO_2$ materials can be alternatively represented in a two component "composite" notation as $xLi_2MnO_3(1-x)LiMO_2$. The appearance of small peaks is also attributed to the super lattice ordering of Li and Mn in the transition-metal layers. These superlattice peaks have been observed in XRD patterns of Li_2MnO_3-based oxides [28]. When the Co content of compound increases, these peaks become broad or disappear because the 1:2 ordering of Li and Mn is destroyed by Co substitution. The largest peak at about $2\theta=18°$ is assigned to the diffraction at the (003) plane indicating the layered structure of $Li[Li_{0.2}Co_{0.3}Mn_{0.5}]O_2$. As can also be seen in Fig. 1a, both (006)/(102) and (108)/(110) peaks are well split, suggesting a well-defined layered structure formed in the lattice. The low values of *R* factor, $R=(I_{102}+I_{006})/I_{101}$, relates to the integrated intensities of the corresponding well resolved peaks of the material confirm their hexagonal ordering. The lower the *R* factor, the better

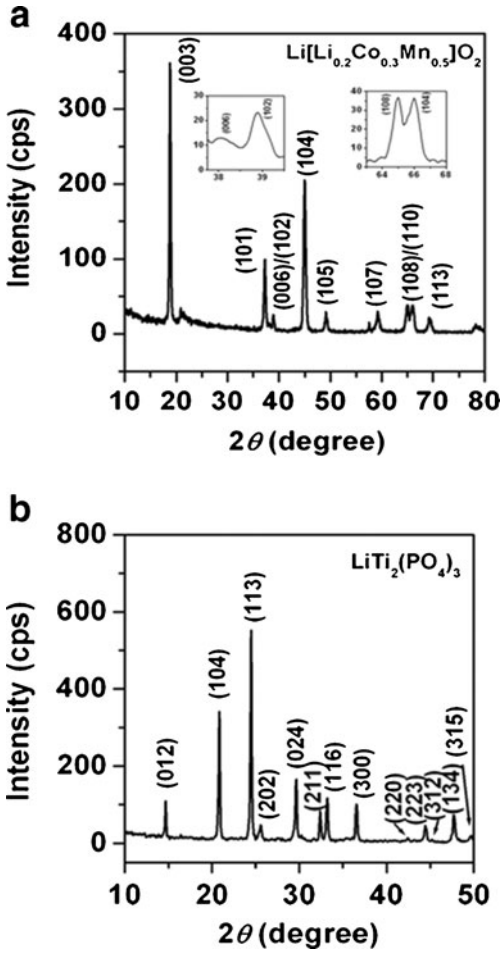

Fig. 1 XRD pattern of **a** $Li[Li_{0.2}Co_{0.3}Mn_{0.5}]O_2$ **b** $LiTi_2(PO_4)_3$ synthesized by RAPET method

is the hexagonal ordering. In general, the integrated intensity ratio (*R*) of the (003) to (104) lines in the XRD patterns can be used to denote the degree of cation mixing in the Li layers of these materials. If the *R* value is >1.2, the cation mixing could be considered to be negligible. In the XRD pattern of $Li[Li_{0.2}Co_{0.3}Mn_{0.5}]O_2$ sample, the relative intensity ratio of the (003) to (104) lines is about 1.7, indicating no pronounced cation mixing and thereby the electrochemical activity of these cathode materials in terms of capacity and rates of lithium ion intercalation–deintercalation is to be very good. We conclude from this XRD results that there are no remarkable impurities in the material obtained and Co^{3+} and Mn^{4+} ions are compatible in the layered hexagonal structure and pure phase solid solutions were obtained. We can assume that Li is in the 3*a* sites, Co^{3+}, Mn^{4+} and Li^+, are in the 3*b* sites, and oxygen is in the 6*c* sites. Since the radii of Co^{3+} (0.54 Å) and Mn^{4+} (0.53 Å) are much smaller than that of Li^+ (0.76 Å), no Co^{3+}, Mn^{4+} are expected to be in the 3*a* Li sites. From the Rietveld analysis, Park et al. [30] have reported that both *a* and *c* parameters decreased linearly with an increase in Co content. As the Co content increases,

Co^{3+} replaced the Li^+ and Mn^{4+} ions in the 3*b* sites and resulted in the decreased lattice parameter. The effect of Mn^{4+} substitution by Co^{3+} is limited due to small difference of ionic radii between these ions. Hence the decrease in the crystal parameter can be attributed to the substitution of Li^+ at 3*b* sites by Co^{3+} which is an evidence for the existence of excess Li^+ at 3*b* sites. Figure 1b shows the XRD patterns of the $LiTi_2(PO_4)_3$ material synthesized by RAPET method. The sample prepared was phase pure according to the XRD pattern. The XRD peaks can be indexed in the rhombohedral crystal system (space group *R3c*).

Cyclic voltammetry

Before testing the given cathode material in an aqueous electrolyte, the stability of the electrode in aqueous media and the safe potential window has to be established. This consideration is necessary, because there are possibilities of oxygen and hydrogen evolution during deintercalation (anodic scan) and intercalation (cathodic scan), respectively. Furthermore, the possibility of dissolution of the electrode material in the aqueous electrolyte cannot be ignored. In the present study, the stability and the safe potential range of $Li[Li_{0.2}Co_{0.3}Mn_{0.5}]O_2$ electrode in aqueous media are evaluated based on the following assumptions [25]: (1) The standard potential of Li^+/Li in non-aqueous electrolyte is the same as that in aqueous electrolytes. (2) The lithium ion intercalation–deintercalation potential widow of $Li[Li_{0.2}Co_{0.3}Mn_{0.5}]O_2$ in aqueous solution can be deduced from the CV curves of this compound in non-aqueous electrolyte. CV of $Li[Li_{0.2}Co_{0.3}Mn_{0.5}]O_2$ in non-aqueous electrolyte (discussed later) shows the potential ranges of lithium intercalation and deintercalation are about 3.45−3.70 and 3.60−4.00 V vs. Li^+/Li, respectively. According to the above assumptions (1) and (2), the corresponding voltage scale vs. SCE for lithium intercalation and deintercalation in aqueous electrolyte is in the safe potential window without oxygen and hydrogen evolution. Furthermore, the electrochemical behavior of $LiCoO_2$, the active component of $Li[Li_{0.2}Co_{0.3}Mn_{0.5}]O_2$, in aqueous electrolyte is already reported [31]. On the basis of the above evidences, we conclude that $Li[Li_{0.2}Co_{0.3}Mn_{0.5}]O_2$ is stable in the aqueous electrolyte within the potential limits of our experiment.

Figure 2a shows the cyclic voltammogram of $Li[Li_{0.2}Co_{0.3}Mn_{0.5}]O_2$ prepared by RAPET method in 2 M Li_2SO_4 aqueous solution at a scan rate of 0.1 mV s^{-1} between 0.0 and 1.2 V. The CV indicate structural changes of $Li[Li_{0.2}Co_{0.3}Mn_{0.5}]O_2$ in the potential region 0.0–1.2 V. There are three pairs of anodic and cathodic peaks located at 0.66/0.63 V, 0.81/0.79 and 0.92/0.91 V, corresponding to deintercalation and intercalation of lithium ions from/into

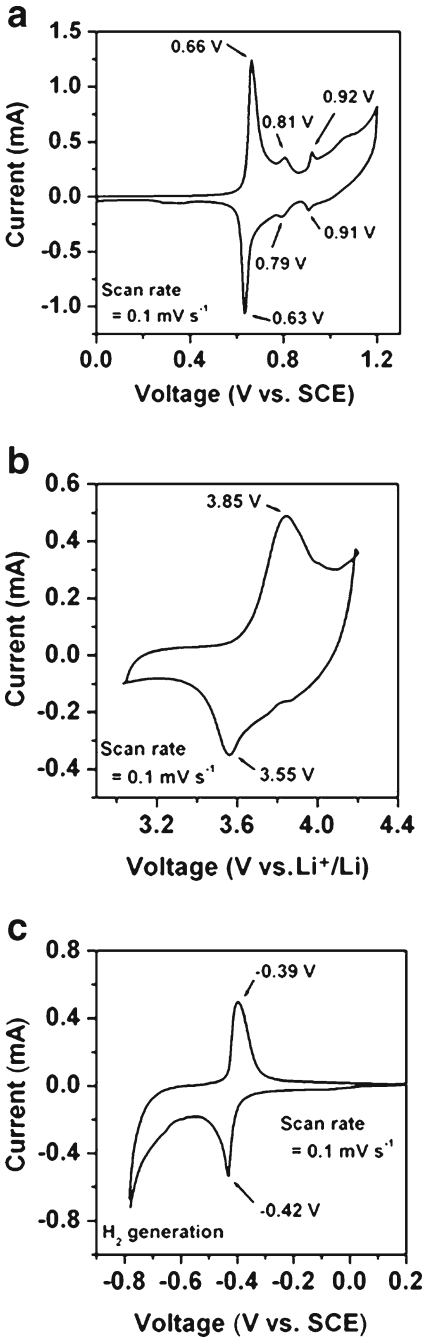

Fig. 2 CV of $Li[Li_{0.2}Co_{0.3}Mn_{0.5}]O_2$ electrode in **a** 2 M Li_2SO_4 aqueous electrolyte; **b** 1 M $LiAsF_6$/EC+DMC; **c** CV of $LiTi_2(PO_4)_3$ electrode in 2 M Li_2SO_4 (scan rate=0.1 mV s^{-1})

$Li[Li_{0.2}Co_{0.3}Mn_{0.5}]O_2$ electrode in accordance with the following equations.

$$\text{Deintercalation}: \ Li[Li_{0.2}Co_{0.3}Mn_{0.5}]O_2 \rightarrow Li_{1-x}[Li_{0.2}Co_{0.3}Mn_{0.5}]O_2 + x\,Li^+ + xe^- \quad (1)$$

$$\text{Intercalation}: \ Li_{1-x}[Li_{0.2}Co_{0.3}Mn_{0.5}]O_2 + x\,Li^+ + x\,e^- \rightarrow Li[Li_{0.2}Co_{0.3}Mn_{0.5}]O_2 \quad (2)$$

The anodic peaks appear due to the oxidation of cobalt ions from Co^{3+} to Co^{4+} accompanied by the deintercalation of equal number of lithium ions. The cathodic peaks are due to the reduction of cobalt ions accompanied by the intercalation of lithium ions. As Li_2MnO_3 component in $Li[Li_{1/3-2x/3}Mn_{2/3-x/3}Co_x]O_2$ is electrochemically inactive the oxidation state of manganese remains as 4+ during intercalation–deintercalation process. Hence, Li_2MnO_3 contains only Mn^{4+} ions, and there are no crystallographic sites available for additional lithium intercalation. The first redox couple at 0.66/0.63 V is related to the existence of a two-phase domain of $Li[Li_{0.2}Co_{0.3}Mn_{0.5}]O_2$; the two small pairs of shoulder-like redox peaks at 0.81/0.79 and 0.92/0.91 V correspond to the presence of a distortion due to an interslab lithium/vacancy ordering. These measurements indicate a sequence of three distinct phase changes occurring as the amount of Li is electrochemically varied between 1 and 0.4 $\{Li[Li^{+}_{0.2}Co^{3+}_{0.3}Mn^{4+}_{0.5}]O_2 \rightarrow Li_{0.6}[Li^{+}_{0.2}Co^{4+}_{0.3}Mn^{4+}_{0.5}]O_2 + 0.4Li\}$. The cyclic voltammogram in Fig. 2a does not exhibit any current peak due to the oxygen evolution reaction, it is inferred that the oxygen evolution does not seriously occur, and at the same time its contribution to the measured current transient is negligibly small. This shows that it is possible to remove lithium ions from the material before the evolution of oxygen. In other words, it is quite reasonable to say that the reduction and oxidation of water does not crucially influence the lithium transport kinetics through the electrode. Thus, it is possible to use the prepared $Li[Li_{0.2}Co_{0.3}Mn_{0.5}]O_2$ as cathode material in the aqueous solution without much oxygen evolution.

The most important feature of the voltammetric peak in our study is their relatively narrow width; the corresponding half-height width is very close to 40 mV instead of 90 mV for one-electron Nernstian reaction. These narrow peaks may be understood if we take into account the possibility of an attractive interaction between the inserted species at their sites. The intercalated lithium ions tighten the $Li[Li_{0.2}Co_{0.3}Mn_{0.5}]O_2$ layers together, resulting in the formation of clusters which can be considered as charge transfer between lithium and the transition metal oxide layers. Hence the intercalation process can be explained by taking into account the possible attractive interaction of the inserted species in terms of the Frumkin-type intercalation isotherm as well as non-equilibrium charging of both the Li|composite and composite|solution interfaces, i.e., the isotherm which is used to model the surface accumulation–consumption process can also describe the intercalation process which occurs in the bulk. The main difference between the intercalation process and adsorption phenomena at interfaces is: for the former case, the bulk concentration is multiplied by the thickness of the layer for the current, whereas for the latter case the current is simply proportional to the surface concentration of the adsorbate. Hence, the adsorption isotherm can be used to describe intercalation phenomena and they may be called intercalation isotherm [32].

Figure 2b shows the CV profile of $Li[Li_{0.2}Co_{0.3}Mn_{0.5}]O_2$ obtained in the organic electrolyte at a scan rate of 0.1 mV s^{-1} using lithium foil as counter and reference electrodes. The cell was cycled in the range from 3.0 to 4.2 V (vs. Li/Li^{+}). A pair of redox peaks at 3.85 and 3.55 V which correspond to the lithium ion deintercalation–intercalation are observed. It can be seen clearly that in the non-aqueous solution the current response of the redox reaction is much lower than that in the aqueous electrolyte solution due to the low ionic conductivity of organic-based solutions. The solvation of lithium ions in the organic solvent with high dipole moment and the resistance offered by the surface layer for lithium ion migration will have a retardation effect on the kinetics of lithium ion insertion. Furthermore, it can be seen that the electrode polarization increases significantly in the organic electrolyte so that the shoulder-like peaks overlap with each other and are less pronounced. In the aqueous solution the smaller peaks appear due to the low electrode polarization.

Figure 2c shows the CV of $LiTi_2(PO_4)_3$ anode in 2 M Li_2SO_4 at a scan rate of 0.1 mV s^{-1}. $LiTi_2(PO_4)_3$ exhibits lithium intercalation and deintercalation potentials of −0.42 and −0.39 V, respectively. Since hydrogen evolution was observed at a more negative potential, it becomes clear that $LiTi_2(PO_4)_3$ can be used as anode in combination with $Li[Li_{0.2}Co_{0.3}Mn_{0.5}]O_2$ cathode in aqueous electrolyte solutions without much hydrogen evolution.

Effect of electrolyte

Aqueous electrolytes present many advantages over non-aqueous systems. If the electrolyte is mainly absorbed in the separators, and the quantity of electrolyte is suitably adapted, aqueous electrolyte batteries may be operated in a sealed, maintenance-free condition. During over charge, oxygen produced at the positive electrode will then diffuse through the separators and can be reduced to water at the negative electrode. This so called oxygen-cycle renders the battery tolerant to overcharge. Water is an ideal electrolyte solvent, in that the decomposition products, hydrogen and oxygen, will not contaminate the electrolyte. Figure 3a shows the cyclic voltammograms of $Li[Li_{0.2}Co_{0.3}Mn_{0.5}]O_2$ electrode in various aqueous electrolyte solutions containing different lithium salts with a scan rate of 0.1 mV s^{-1}. Even though, all these voltammograms are characterized by a pair of redox peaks, there is a pronounced difference in the behavior of $Li[Li_{0.2}Co_{0.3}Mn_{0.5}]O_2$ electrode with respect to peak current and potential in different electrolytes. With 2 M Li_2SO_4 solution, the peaks are sharp and well defined, indicating that the faradaic reaction involving the intercalation–deintercalation of lithium ions is much more facile in

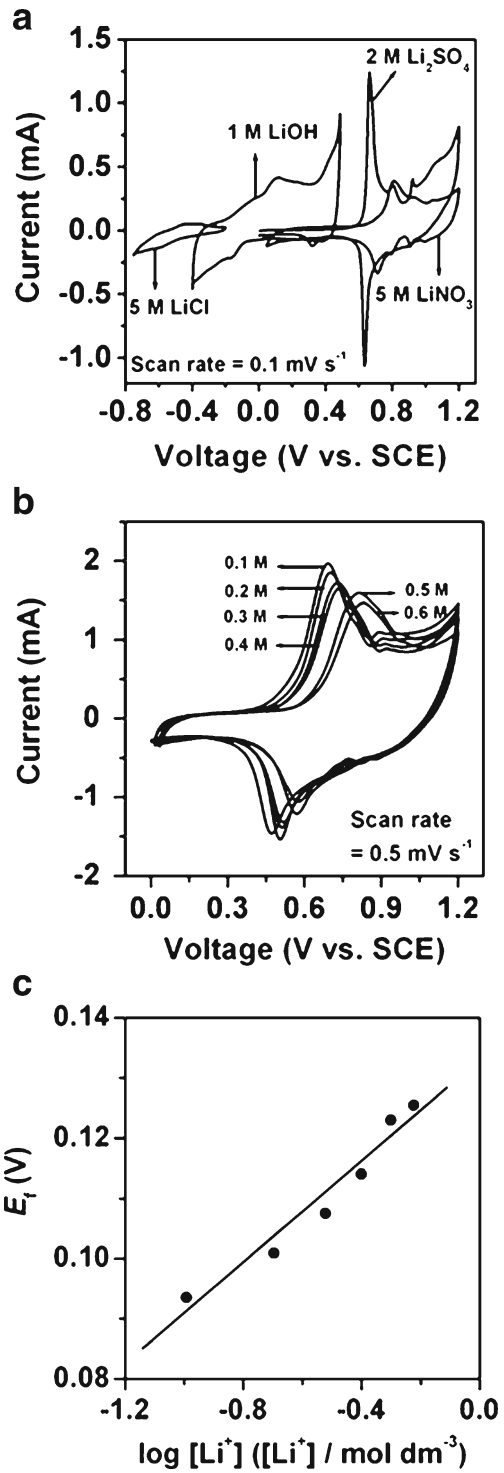

Fig. 3 CV of $Li[Li_{0.2}Co_{0.3}Mn_{0.5}]O_2$ electrode in **a** different electrolytes and **b** different concentrations of Li_2SO_4 electrolyte. **c** Plot of formal potential, E_f, vs. log[Li^+] in Li_2SO_4 electrolytes

Li_2SO_4 than in other electrolytes. In 5 M $LiNO_3$ solution, the peaks appear at a more positive potentials, providing a wider potential window when combined with $LiTi_2(PO_4)_3$, but a poor current response. Both in LiOH and LiCl solutions, the redox peaks are at more negative potentials with lower peak currents, indicating unfavorable intercalation–deintercalation kinetics of lithium ions with these electrolytes. The shift of the electrode potentials toward the negative direction indicates a decrease in the free energy for the redox reaction. On the basis of above inferences, we concluded that Li_2SO_4 is the best electrolyte to study the electrochemical behavior of $Li[Li_{0.2}Co_{0.3}Mn_{0.5}]O_2$ electrode in aqueous solution. The better performance of the system in a particular electrolyte has many folds. The chemical stability of anions of various lithium salts may have an effect on the electrochemical behavior of the electrode. The kinetics of lithium ion intercalation–deintercalation are also affected by many other characteristics of the electrolyte such as pH, viscosity, ionic conductivity, lithium ion transference number, dipole moment, solvation of ions, compatibility of the electrolyte with other cell components. Further investigations are needed to elucidate the details.

Identification of cation

It is necessary to identify the cation, which deintercalate/intercalate from/into $Li[Li_{0.2}Co_{0.3}Mn_{0.5}]O_2$ compound upon the redox reaction. To solve this problem, we have recorded the CVs of the electrode at different concentrations of Li_2SO_4 aqueous electrolytes. Figure 3b shows the cyclic voltammograms of $Li[Li_{0.2}Co_{0.3}Mn_{0.5}]O_2$ electrode with a scan rate of 0.1 mV s^{-1} in various concentrations of Li_2SO_4 aqueous electrolytes. If we suppose that the deintercalating–intercalating cation is lithium ion, then Eqs. (1) and (2) represent the corresponding reactions. According to Nernst law, the oxidation (1) and reduction (2) reactions should follow the dependence of the formal potential, $E_f=(E_{p,a}+E_{p,c})/2$ (where $E_{p,a}$ and $E_{p,c}$ are the anodic and cathodic peak potentials, respectively) on the activity of the lithium ion, a_{Li+}:

$$E_f = E^\circ + \log a_{Li+} \tag{3}$$

i.e., the formal potential of the redox reaction should be directly proportional to the logarithm of lithium ion activity in the Li_2SO_4 electrolyte solution. Figure 3c shows the plot of E_f vs. log [Li^+] at various concentrations of alkali electrolyte solutions. The straight line with a positive slope confirms that, the redox peaks on the CVs of $Li[Li_{0.2}Co_{0.3}Mn_{0.5}]O_2$ in Li_2SO_4 aqueous electrolytes can be attributed to the deintercalation–intercalation of lithium ions.

Effect of scan rate

To investigate the influence of scan rate on the redox behaviors of $Li[Li_{0.2}Co_{0.3}Mn_{0.5}]O_2$ electrode in Li_2SO_4 aqueous electrolyte, its CV curves at different scan rates were recorded and are shown in Fig. 4a. Although the curved shape of the anodic and cathodic peak was almost

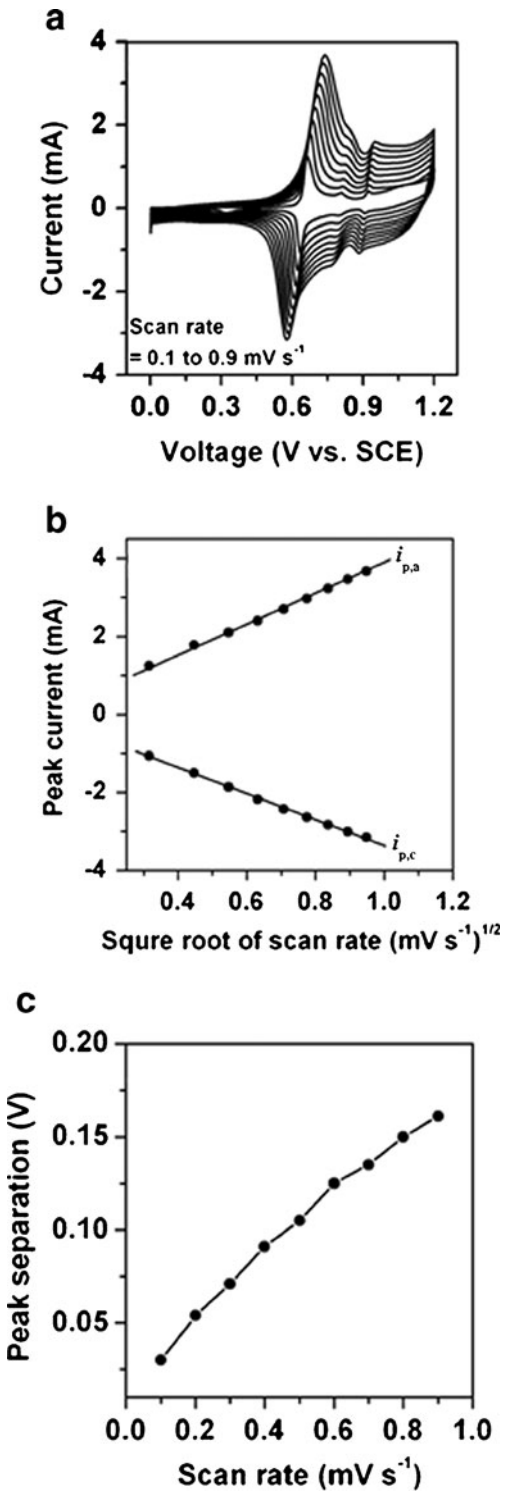

Fig. 4 **a** CV of $Li[Li_{0.2}Co_{0.3}Mn_{0.5}]O_2$ electrode in 2 M Li_2SO_4 at different scan rates. **b** Relationship between peak currents and square root of scan rates. **c** Effect of scan rate on the peak separation

symmetrical, the peak potential difference ($E_{p,a}-E_{p,c}$) between the two peaks increased with scan rate as shown in Table 1. A combination of Butler–Volmer equation with non-Nernstain intercalation isotherms provides a basis for performing numerical simulation of the voltammetric response, thus taking into account non-equilibrium phenomena at the electrode–solution interface. It can be seen that the electrode polarization increases as the scan rate increases, and the three couples of redox peaks overlapped with each other and are less pronounced at higher scan rates. The voltammogrm reveals a quasi-equilibrium behavior which is reflected by the separation of the corresponding cathodic and anodic peak potentials. This separation between cathodic and anodic peaks was observed at all scan rates, which suggests that the peak separation during lithium ion intercalation–deintercalation is intrinsic. The slow conversion rate between the solid-state phases for lithium intercalation compounds should be the most probable reason for this observation [33].

Table 1 Peak potential difference ($E_{p,a}-E_{p,c}$) and diffusion coefficient, D calculated from the anodic and cathodic peak currents of CV profiles at different scan rates

Scan rate (mV s^{-1})	($E_{p,a}-E_{p,c}$) (V)	$D\times10^{-8}$ (cm^2 s^{-1}) (anodic)	$D\times10^{-8}$ (cm^2 s^{-1}) (cathodic)
0.1	0.030	1.717	1.256
0.2	0.054	1.756	1.247
0.3	0.071	1.636	1.285
0.4	0.091	1.605	1.311
0.5	0.105	1.613	1.306
0.6	0.125	1.623	1.284
0.7	0.135	1.644	1.276
0.8	0.150	1.660	1.253
0.9	0.161	1.666	1.231

The rate-determining steps of the electrochemical intercalation, on going from high potential scan rate (short experimental time) to low potential scan rate (long time) may change in the following sequence: interfacial charge transfer, planar semi-infinite and finite space solid-state diffusion of the intercalated species and finally the accumulation of these species in the bulk of the electrodes. The dependence of the peak current (I_p) on the potential scan rate (ν) is a major tool to distinguish between these different cases. In the case of semi-infinite diffusion, the peak current, I_p for a redox reaction may be expressed by the *Randles–Sevcik* equation [34]:

$$I_p = 2.69\times10^5 An^{2/3}CD^{1/2}\nu^{1/2} \quad (\text{at } 25^\circ\text{C}). \tag{4}$$

where n is the number of electrons per reaction (one for Li), A is the apparent surface area of the electrode, D is the diffusion coefficient of lithium ion in the solid state and C is the concentration of lithium ions.

It is well known that Eq. 4 was derived for the case of semi-infinite diffusion of redox species whose bulk concentration is not substantially changed during the time of the

experiments. This condition cannot be fulfilled during the lithium intercalation process in $Li[Li_{0.2}Co_{0.3}Mn_{0.5}]O_2$ since CV peaks in Fig. 4a relate to the changes in the bulk concentration of lithium in the cathode material. However, the CV peaks measured at the above mentioned scan rates have a typical semi-infinite diffusion character (a linear dependence of I_p on $\nu^{1/2}$ as seen in Fig. 4b). Thus, in this case, Eq. 4 is applicable as an approximation because at the scan rates used in this study, the amount of charge injected at the peak potential is small compared with the charge involved in the entire redox step, i.e., the concentration of lithium ions at the peak potential is only slightly different from that at the foot of the peak. It is seen that the peak currents are proportional to the square root of the scan rates indicating that the semi-infinite diffusion is valid for these scan rates. The slope of I_p vs. $\nu^{1/2}$ is proportional, according to Eq. 4 to the amount of intercalated lithium ions. Comparison of Eq. 4 with the slopes of the curves in Fig. 4b enables the calculation of effective values of the diffusion coefficient for lithium ions in $Li[Li_{0.2}Co_{0.3}Mn_{0.5}]O_2$ electrode. Table 1 lists these values for all scan rates. However, Eq. 4 is valid only for Nernstian semi-infinite diffusion process. The intercalation process under study is in fact non–Nernstian for the following reasons: (1) there may be a strong attractive interaction between the inserted lithium ions at their sites; and (2) one should take into account the influence of the slow charge transfer rate on the linear sweep voltammetric response. Hence, calculating the diffusion coefficients for lithium ion in $Li[Li_{0.2}Co_{0.3}Mn_{0.5}]O_2$ based on Eq. 4, and Fig. 4b may provide only approximate values. CV is usually used in the study of electrode kinetics only as a qualitative tool which is a basis for designing more precise experiments.

Figure 4c shows the scan rate dependency of the cathodic and anodic peak separation obtained from cyclic voltammograms of $Li[Li_{0.2}Co_{0.3}Mn_{0.5}]O_2$ electrode in 2 M Li_2SO_4 at different scan rates. As expected, the peak separation increases with increase in scan rate as the anodic peaks shift towards a more positive potential and cathodic peaks shift to the negative ones. This could be ascribed to the effect of concentration polarization and may be due to slow electron transfer. Further, at low scan rates, the system may yield reversible waves, while at large scan rates, irreversible behavior is observed, which may make us assume that the electrochemical lithium ion deintercalation–intercalation process changes from being kinetically quasi-reversible to irreversible when scan rate increases from low to high.

Galvanostatic charge–discharge cycling

To study the charge–discharge cycling behavior of the prepared $Li[Li_{0.2}Co_{0.3}Mn_{0.5}]O_2$ electrode, a coin cell was made using $Li[Li_{0.2}Co_{0.3}Mn_{0.5}]O_2$ as cathode and $LiTi_2(PO_4)_3$ as anode in 2 M Li_2SO_4 aqueous solution. The charging and discharging of lithium ion batteries involves lithium ion transfer from one insertion electrode to another one. This transfer can be considered as a topotactic intercalation reaction, meaning that the guest ions occupy the interstitial sites of both crystalline host matrices and that their charging and discharging result in a non uniform concentration profile in the electrodes' bulk, thus separating the coexisting phases with different concentrations of guest ions. The typical charge and discharge curves of $LiTi_2(PO_4)_3$/2 M Li_2SO_4/$Li[Li_{0.2}Co_{0.3}Mn_{0.5}]O_2$ cell in the first cycle at a current density of 0.1 mA cm^{-2} are shown in Fig. 5a. The voltage range was limited from 0.0 to 1.3 V. The clear cutoff voltage provides a charge–discharge voltage range that can avoid the decomposition of water. Obviously, during charging process lithium ions deintercalate from $Li[Li_{0.2}Co_{0.3}Mn_{0.5}]O_2$ and intercalate into $LiTi_2(PO_4)_3$ and reverse process occurs during discharge process in accordance with the following equations:

$$\text{Charge}: Li[Li_{0.2}Co_{0.3}Mn_{0.5}]O_2 + LiTi_2(PO_4)_3 \rightarrow Li_{(1-x)}[Li_{0.2}Co_{0.3}Mn_{0.5}]O_2 + Li_{(1+x)}Ti_2(PO_4)_3 \quad (5)$$

$$\text{Discharge}: Li_{(1-x)}[Li_{0.2}Co_{0.3}Mn_{0.5}]O_2 + Li_{(1+x)}Ti_2(PO_4)_3 \rightarrow Li[Li_{0.2}Co_{0.3}Mn_{0.5}]O_2 + LiTi_2(PO_4)_3 \quad (6)$$

It is clear that their voltage curves are almost similar in shape and both display a voltage plateau at about 0.8 V. Moreover, the cycling behavior of $LiTi_2(PO_4)_3$/2 M Li_2SO_4/$Li[Li_{0.2}Co_{0.3}Mn_{0.5}]O_2$ cell shows that this kind of cell is good in reversible intercalation and deintercalation of lithium ions. The maximum discharge capacity is 90 mA h g^{-1}. The variation of discharge capacity and coulombic efficiency with cycle number is shown in Fig. 5b. After hundred cycles, the charge–discharge efficiency, which is the ratio of the discharge capacity to that of the charge capacity for a given cycle, is about 99 %. This value indicates that almost no side reaction, such as electrolysis of water occurs and that almost the complete deintercalated amount of lithium ions can be intercalated during the succeeding discharge process. This can be ascribed to the good stability of the two electrodes during cycling in the aqueous electrolyte. Because of these attractive results, the influence of the current upon the capacity during cycling was investigated. The results are shown in Fig. 5c. It can be seen that the $Li[Li_{0.2}Co_{0.3}Mn_{0.5}]O_2$ electrode maintained reasonable capacity even at higher currents in these aqueous electrolytic cell. If the capacities of the electrodes are increased to the level in organic electrolytes, this system will have great promise since this kind of battery is very safe for large-scale energy storage. Figure 5c and d shows the charge–discharge and cycling stability curves of Li/1 M $LiAsF_6$/EC +DMC/$Li[Li_{0.2}Co_{0.3}Mn_{0.5}]O_2$ cell at the current density of

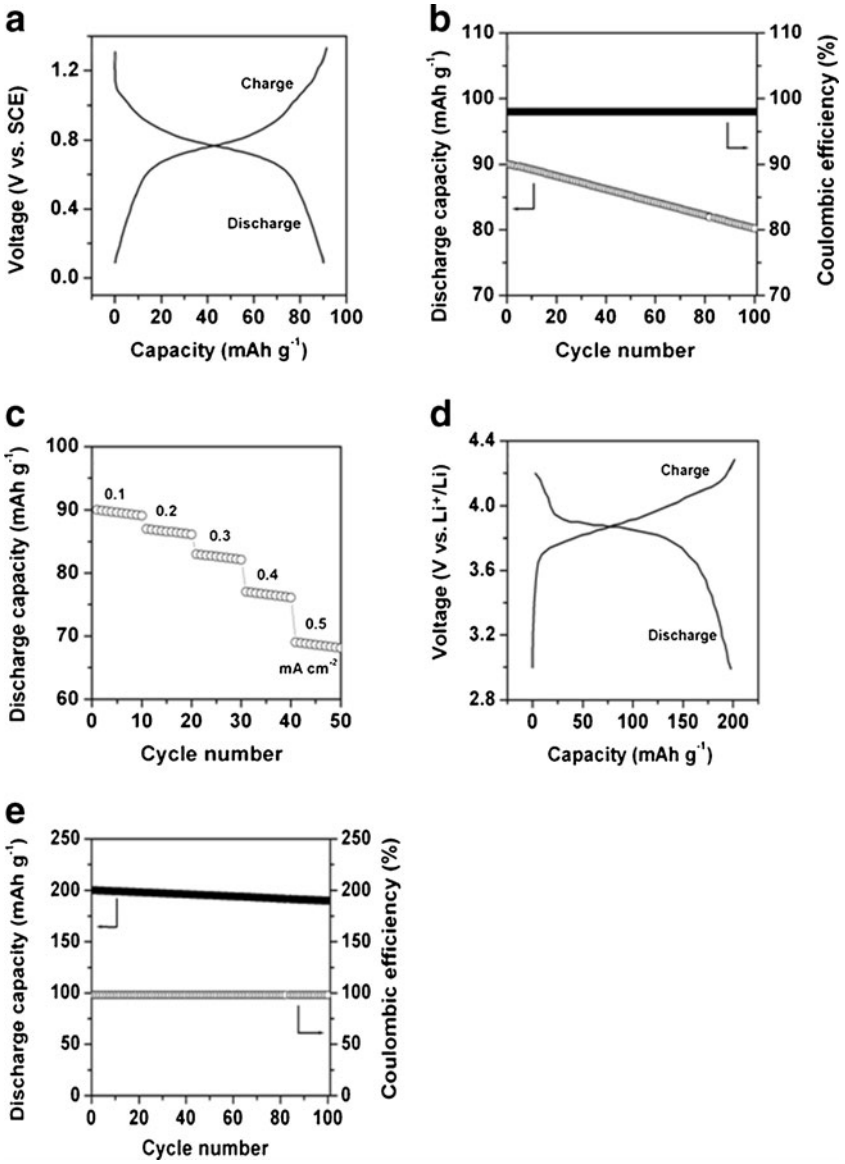

Fig. 5 **a** Charge–discharge curves; **b** cycling behavior at a current density of 0.1 mA cm^{-2}; **c** variation of discharge capacity as a function of current density for $LiTi_2(PO_4)_3$/$Li[Li_{0.2}Co_{0.3}Mn_{0.5}]O_2$ cell in 2 M Li_2SO_4 electrolyte; **d** charge–discharge curves; **e** cycling behavior at a current density of 0.1 mA cm^{-2} of Li/$Li[Li_{0.2}Co_{0.3}Mn_{0.5}]O_2$ cell in non-aqueous electrolyte

0.1 mA cm^{-2} in the potential range 3–4.3 V. The curves are similar to that in aqueous electrolyte except that the capacity in the former is lower than that in the latter. This is due to the lower potential window of aqueous electrolytes. These results clearly show that the charge and discharge behavior in organic electrolytes can be transferred into aqueous solution if the intercalation and deintercalation voltages are within the stable electrochemical window of water. If it is possible to charge the battery cell to a higher voltage without causing the kinetic electrolysis of the aqueous electrolyte, a significantly increased capacity is expected. Nevertheless, this battery system based on a neutral aqueous electrolyte is an interesting alternative in battery research, concerning its cost-effectiveness (non-expensive materials, easy assembling), environmental friendliness, and fundamental safety by avoiding the use of poisonous metals as well as flammable, harmful, acidic or alkaline electrolytes.

Electrochemical impedance studies

The kinetics of lithium ion intercalation process in $Li[Li_{0.2}Co_{0.3}Mn_{0.5}]O_2$ electrode was obtained by electrochemical impedance spectroscopy (EIS). The characteristic impedance spectra and its potential dependence provide important kinetic information on the mechanism of intercalation processes, which cannot be obtained from the CV plots. EIS results obtained with $Li[Li_{0.2}Co_{0.3}Mn_{0.5}]O_2$ electrode in 2 M Li_2SO_4 solution at different potentials during the discharge process in the potential range 0.80–0.50 V are shown in Fig. 6a–c. All Nyquist plots consist of three parts: an arc in the high frequency range, a Warburg-type element in the middle to low frequency range, and an inclining line in the low frequency range. These impedance spectra reflect the nature of overall lithium ion intercalation process. The high frequency range generally corresponds to charge transfer

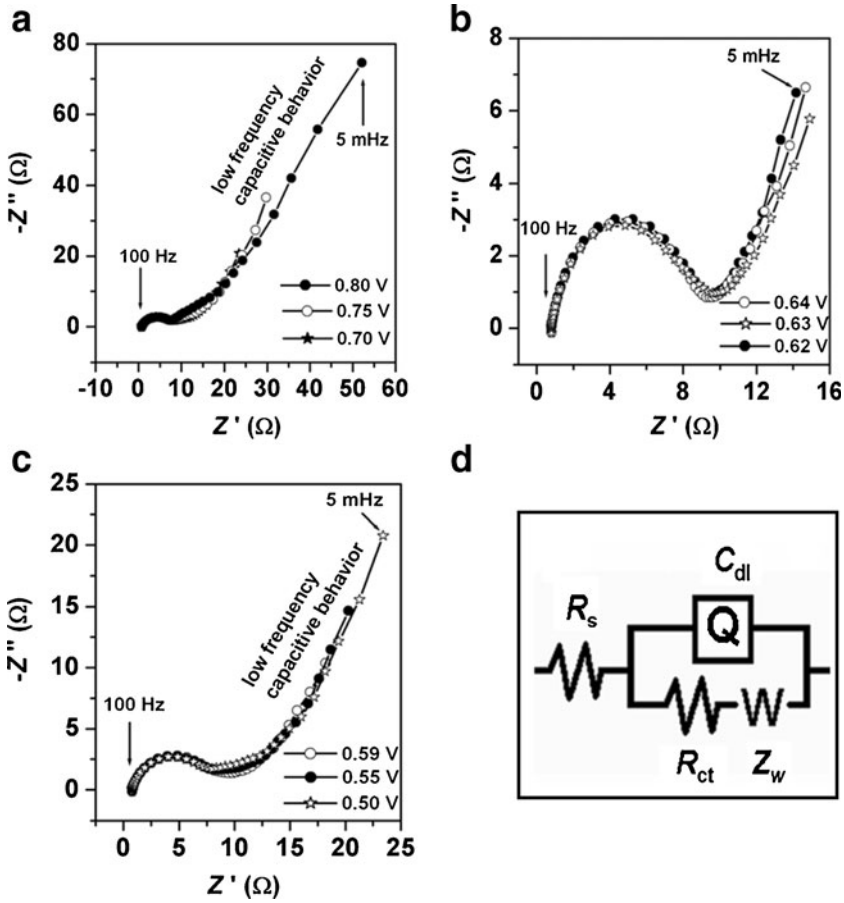

Fig. 6 **a**–**c** Nyquist plots of the $Li[Li_{0.2}Co_{0.3}Mn_{0.5}]O_2$ electrode in 2 M Li_2SO_4 at different discharge voltages; **d** corresponding equivalent circuit

through the electrode/electrolyte interface, the Warburg region is assigned to the diffusion of lithium ions in $Li[Li_{0.2}Co_{0.3}Mn_{0.5}]O_2$ that is often described as finite space or restricted diffusion, while the sloping line reflects a capacitive behavior of the electrode. In accordance with the results obtained an equivalent circuit, as shown in Fig. 6d, is proposed to fit the impedance spectra. In this equivalent circuit, R_s represents the ohmic resistance of the electrolyte solution which is related to the distance of the high frequency intercept with the real axis to the axis origin, R_{ct} is the resistance of the charge transfer reaction, Q is the capacitance of the electrode–electrolyte double layer and Z_w is the Warburg impedance. To achieve better fitting results, pure capacitor in the equivalent circuit is replaced by constant phase element (CPE, Q). CPE is used when impedance spectra exhibits low frequency dispersion. A Nyquist plot of similar compounds in non aqueous electrolytes consists of two semicircles: a potential independent semicircle in the high frequency region and a strongly potential dependent larger semicircle in the medium frequency region [35]. The high-frequency semicircle reflects the resistance for lithium ion migration through the surface film and film capacitance of the electrode. The absence of this region may be due to high rate performance (short diffusion path) and/or a small resistance offered by the surface layer for the migration of lithium ions which does not resist the diffusion of lithium ions.

Figure 6a shows a family of Nyquist plots related to lithium ion intercalation into the layered phase before the CV peak potential. The main feature of this region is that it exhibits semicircles (high frequency semicircle [HFS]) which are not complete towards the low frequencies; followed by a sloping, low frequency capacitive line. In these curves the length of capacitive line decreases with the decrease in potential, indicating that the interfacial capacitance between the electrode and the electrolyte decreases with the decrease in potential. Figure 6b shows the Nyquist plots in the vicinity of CV peak potentials (i.e., during the course of lithium ion intercalation). In this region, a semicircle rather than an arc appears with a decrease in the sloping capacitive behavior. The low frequency capacitive lines disappear and the Warburg behavior dominates the low frequency region of the spectra, as diffusion is the main process after high frequency relaxation. In this figure, we see a curve with a minimum at 0.63 V when all the points related to the $-Z''$ values at 5 MHz, i.e., the lowest frequency used in this study are compared with each other. The potential of the above minimum corresponds to the potential of the CV peak. Thus, the low-frequency impedance measurements are in qualitative agreement with the CV characterizations of the same

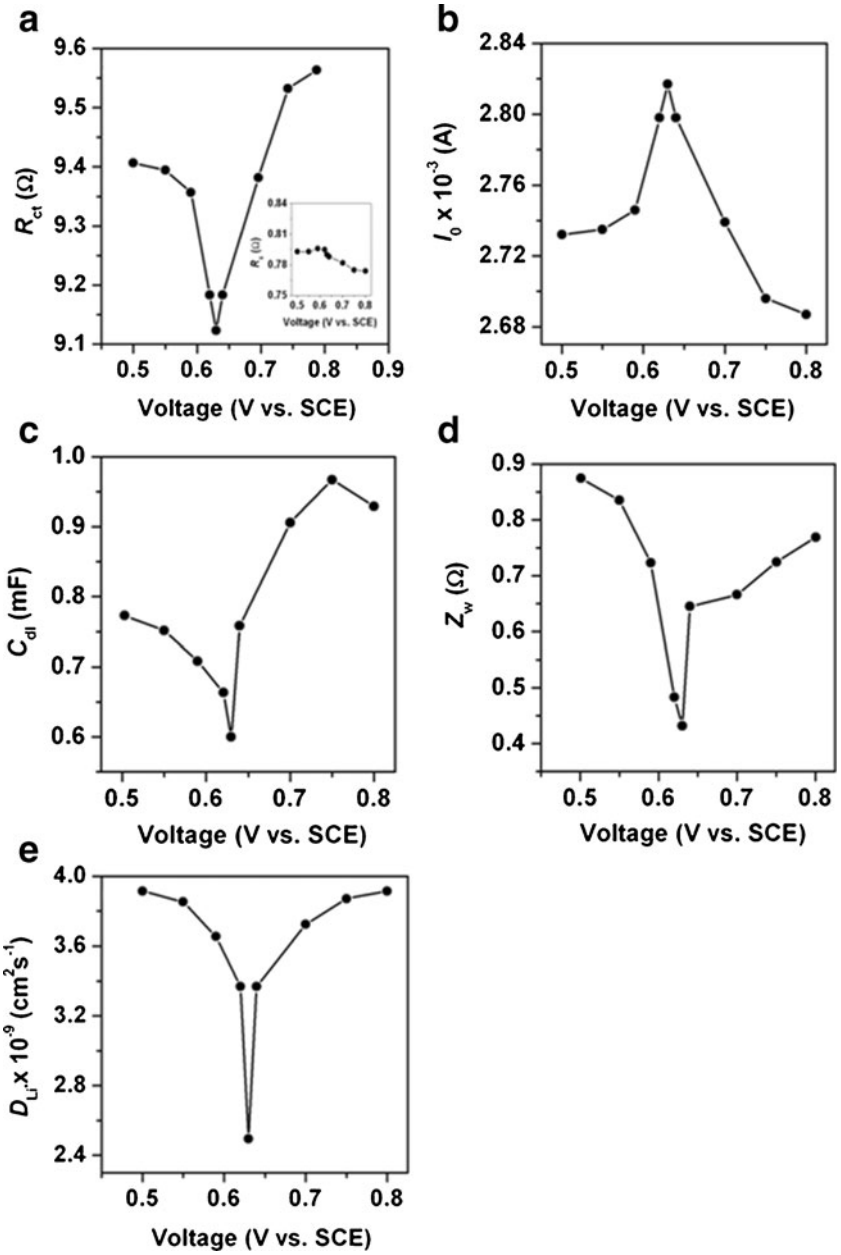

Fig. 7 Evaluated impedance parameters according to the equivalent circuit in Fig. 6d as a function of electrode potential during lithium intercalation process

electrode, i.e., intercalation capacitance (C_{int}) for lithium intercalated hosts is inversely proportional to the imaginary part of the impedance ($-Z''$) at very low frequencies ($\omega \rightarrow 0$), $C_{int}=(-\omega Z'')^{-1}$, where ω is the angular velocity of the ac

Table 2 Evaluated impedance parameters according to the equivalent circuit in Fig. 6d as a function of electrode potential during the lithium intercalation process

E (V)	R_s (Ω)	R_{ct} (Ω)	$I_o \times 10^{-3}$ (A)	C_{dl} (mF)	Z_w (Ω)	$D_{Li+} \times 10^{-9}$ (cm^2 s^{-1})
0.50	0.793	9.406	2.732	0.772	0.874	3.915
0.55	0.793	9.394	2.735	0.751	0.835	3.853
0.59	0.796	9.356	2.746	0.708	0.723	3.654
0.62	0.795	9.183	2.798	0.663	0.483	3.368
0.63	0.790	9.123	2.817	0.600	0.432	2.495
0.64	0.788	9.183	2.798	0.758	0.645	3.368
0.70	0.782	9.381	2.739	0.906	0.666	3.724
0.75	0.775	9.532	2.696	0.967	0.724	3.871
0.80	0.774	9.563	2.687	0.929	0.769	3.915

response. Figure 6c shows the impedance spectra measured at potentials after the CV peak, i.e., towards the end of lithium intercalation process. In this region, the capacitive line begins to appear indicating the end of lithium ion intercalation.

Figure 7 shows the variation of kinetic parameters of the equivalent circuit from the experimental impedance data of the $Li[Li_{0.2}Co_{0.3}Mn_{0.5}]O_2$ electrode during lithium ion intercalation. Solution resistance, R_s stays constant at about 0.8 Ω as expected because solution composition and thus conductance do not change during intercalation process. R_{ct} decreases with the potential and reaches a minimum at 0.63 V, and then increases (Fig. 7a). From the CV curves, it can be seen that at 0.63 V the reduction reaction shows a peak implying favorable kinetic conditions for lithium intercalation. The Butler–Volmer equation can be linearized when the amplitude of the potential perturbation signal is less than 10 mV. The exchange current I_0 is related to R_{ct} according to the following equation:

$$I_0 = RT/nFR_{ct} \tag{7}$$

where R is the gas constant, T is the absolute temperature, n is the number of the electrons and F is Faraday constant. Figure 7b shows the variation of I_0 with discharge voltage. I_0 increases with the potential and reaches a maximum at 0.63 V, when the charge transfer resistance is lowest, and then decreases. Double layer capacitance, C_{dl}, decreases slightly at first with the voltage, perhaps due to a conceivable activation process since there is no passivating film on the surface of the electrode, and then increases (Fig. 7c). Since C_{dl} represents the double layer capacitance of the electrode–solution interface, it is a function of electrode potential and does not behave like a simple capacitor, whose capacity is independent of the applied voltage. Figure 7d shows that Warburg impedance, Z_w decreases gradually during the intercalation of lithium ions into $Li[Li_{0.2}Co_{0.3}Mn_{0.5}]O_2$ and then reaches to the minimum at 0.63 V. Subsequently, the values of Z_w increases gradually up to the maximum.

The diffusion coefficient of lithium ion, D_{Li+} can be calculated from the impedance data by analyzing the low frequency Warburg contribution according to the following equation:

$$D = R^2T^2/2A^2n^4F^4C^2\sigma^2 \tag{8}$$

where R is the gas constant, T is the absolute temperature, n is the number of the electrons, A is the surface area, F is Faraday constant, C is concentration and σ is the Warburg factor which is related to the real part of impedance (Z_{re}) as

$$Z_{re} = R_s + R_{ct} + \sigma\omega^{-1/2} \tag{9}$$

where ω is the angular frequency of the small-amplitude ac voltage.

Figure 7e shows the variation of D_{Li+}, calculated by using Eq. 8, with applied potential. It can be seen that the diffusion coefficient of lithium ion gradually decreases and reaches a minimum at 0.63 V and then increases. One can see that the potential of minima on the D_{Li+} vs. E correspond well with the potential of cathodic CV peak, as expected. As already reported, in accordance with the view on the influence of short-range interactions on lithium ion diffusion, D_{Li+} vs. E plots calculated from many lithium insertion electrodes have sharp minima at the slow scan rate CV peak potentials [36]. The values of kinetic parameters measured from the impedance data during the discharge process are summarized in Table 2.

Conclusions

$Li[Li_{0.2}Co_{0.3}Mn_{0.5}]O_2$ cathode materials were synthesized by a simple, time- and energy-saving method called RAPET. CV measurements show that the electrode is stable in both aqueous and non-aqueous electrolytes. An aqueous rechargeable lithium battery has been constructed with $Li[Li_{0.2}Co_{0.3}Mn_{0.5}]O_2$ as the positive electrode and $LiTi_2(PO_4)_3$ as the negative electrode based on intercalation and deintercalation of lithium ions during charge and discharge process and is compared with that in a non aqueous solution. It is an interesting alternative battery in light of its cost, environmental friendliness, and fundamental safety by avoiding the use of poisonous metals as well as flammable, harmful electrolytes. $Li[Li_{0.2}Co_{0.3}Mn_{0.5}]O_2$ might be a candidate cathode material which can compete or even surpass the performances of the materials in the common rechargeable battery systems.

Acknowledgements The authors gratefully acknowledge the financial support from the Department of Science and Technology, Government of India. The authors wish to thank Sri. A.V.S. Murthy, honorary secretary, Rashtreeya Sikshana Samiti Trust, Bangalore and Dr. P. Yashoda, Principal, SSMRV Degree College, Bangalore, for their support and encouragement. The authors also thank the Department of Chemistry, St. Joseph's College, Bangalore, for the XRD data.

References

1. Chen R, Whittingham MS (1997) J Electrochem Soc 144:L64–L67
2. Armstrong AR, Bruce PG (1996) Nature 381:499–500
3. Stoyanova R, Zhecheva E, Zarkova L (1994) Solid State Ionics 73:233–240
4. Armstrong AR, Gitzendanner R, Robertson AD, Bruce PG (1998) Chem Commun 17:1833–1834
5. Numata K, Yamanaka S (1999) Solid State Ionics 118:117–120
6. Caurant D, Baffier N, Bianchi V, Gregoire G, Bach S (1996) J Mater Chem 6:1149–1155
7. Yoshio M, Yamato K, Itoh J, Noguchi H, Okada M, Mouri T (1994) Electrochem Soc Proc 94–28:251

8. Nitta Y, Okamura K, Haraguchi K, Kobayashi S, Ohta A (1995) J Power Sources 54:511–515
9. Armstrong AR, Paterson AJ, Robertson AD, Bruce PG (2002) Chem Mater 14:710–719
10. Armstrong AR, Robertson AD, Bruce PG (1999) Electrochim Acta 45:285–294
11. Zhang F, Whittingham MS (2000) Electrochem Solid-State Lett 3:309–311
12. Thackeray MM, Johnson CS, Vaughey JT, Li N, Hackney SA (2005) J erMat Chem 15:2257–2267
13. Lu Z, Dahn JR (2002) J Electrochem Soc 149:A815–A822
14. He W, Qian J, Cao Y, Ai X, Yang H (2012) RSC Adv 2:3423–3429
15. Armstrong AR, Holzapfel M, Novak P, Johnson CS, Kang SH, Thackeray MM, Bruce PG (2006) J Am Chem Soc 128:8694–8698
16. Xu B, Fell CR, Chi MF, Meng YS (2011) Energy Environ Sci 4:2223–2233
17. Ito A, Li D, Sato CY, Arao M, Watanabe M, Hatano M, Horie H, Ohsawa Y (2010) J Power Sources 195:567–573
18. Gao J, Manthiram A (2009) J Power Sources 191:644–647
19. Arunkumar TA, Alvarez E, Manthiram A (2008) J Mater Chem 18:190–198
20. Al-Hallaj S, Selman JR (2002) J Power Sources 110:341–348
21. Nelson P, Bloom I, Amine K, Henriksen G (2002) J Power Sources 110:437–444
22. Kohler J, Makihara H, Uegaito H, Inoue H, Toki M (2000) Electrochim Acta 46:59–65
23. Li W, Dahn JR, Wainwright D (1994) Science 264:1115–1118
24. Zhang M, Dahn JR (1996) J Electrochem Soc 143:2730–2735
25. Mi CH, Zhang XG, Li HL (2007) J Electroanal Chem 602:245–254
26. Kim Y, Hong Y, Kim MG, Cho J (2007) Electrochem Commun 9:1041–1046
27. Santhanam R, Rambabu B (2009) Int J Electrochem Sci 4:1770–1778
28. Kang SH, Sun YK, Amine K (2003) Electrochem Solid-State Lett 6:A183–A186
29. Zhao Y, Zhao C, Feng H, Sun Z, Xiab D (2011) Electrochem Solid-State Lett 14:A1–A5
30. Park YJ, Hong YS, Wu X, Kim MG, Ryu KS, Chang SH (2004) J Electrochem Soc 151:A720–A727
31. Wang GJ, Qu QT, Wang B, Shi Y, Tian S, Wu YP, Holze R (2009) Electrochim Acta 54:1199–1203
32. Vorotyntsev MA, Daikhin LI, Levi MD (1992) J Electroanal Chem 332:213–235
33. Levi MD, Aurbach D (1997) J Electroanal Chem 421:79–88
34. Bard AJ, Faulkner LR (1980) Electrochemical methods. Wiley, New York
35. Lin B, When Z, Gu Z, Huang S (2008) J Power Sources 175:564–569
36. Levi MD, Aurbach D (1997) J Phys Chem B 101:4641–4647